photonics

Article

An Indoor Visible Light Positioning System for Multi-Cell Networks

Roger Alexander Martínez-Ciro [1,*], Francisco Eugenio López-Giraldo [1], José Martín Luna-Rivera [2] and Atziry Magaly Ramírez-Aguilera [3]

1 Facultad de Ingenierías, Instituto Tectonológico Metropolitano (ITM), Calle 54A No. 30-01, Barrio Boston, Medellin 050012, Colombia; franciscolopez@itm.edu.co
2 Facultad de Ciencias, Universidad Autónoma de San Luis Potosí (UASLP), Av. Chapultepec 1570, San Luis Potosi 78295, Mexico; mlr@fciencias.uaslp.mx
3 Unidad Académica de Ingeniería Eléctrica, Universidad Autónoma de Zacatecas (UAZ), Campus Siglo XXI, Zacatecas 98160, Mexico; atziry.ra@uaz.edu.mx
* Correspondence: rogermartinez@itm.edu.co; Tel.: +57-460-0727 (ext. 5586)

Abstract: Indoor positioning systems based on visible light communication (VLC) using white light-emitting diodes (WLEDs) have been widely studied in the literature. In this paper, we present an indoor visible-light positioning (VLP) system based on red–green–blue (RGB) LEDs and a frequency division multiplexing (FDM) scheme. This system combines the functions of an FDM scheme at the transmitters (RGB LEDs) and a received signal strength (RSS) technique to estimate the receiver position. The contribution of this work is two-fold. First, a new VLP system with RGB LEDs is proposed for a multi-cell network. Here, the RGB LEDs allow the exploitation of the chromatic space to transmit the VLP information. In addition, the VLC receiver leverages the responsivity of a single photodiode for estimating the FDM signals in RGB lighting channels. A second contribution is the derivation of an expression to calculate the optical power received by the photodiode for each incident RGB light. To this end, we consider a VLC channel model that includes both line-of-sight (LOS) and non-line-of-sight (NLOS) components. The fast Fourier transform (FFT) estimates the powers and frequencies of the received FDM signal. The receiver uses these optical signal powers in the RSS-based localization application to calculate the Euclidean distances and the frequencies for the RGB LED position. Subsequently, the receiver's location is estimated using the Euclidean distances and RGB LED positions via a trilateration algorithm. Finally, Monte Carlo simulations are performed to evaluate the error performance of the proposed VLP system in a multi-cell scenario. The results show a high positioning accuracy performance for different color points. The average positioning error for all chromatic points was less than 2.2 cm. These results suggest that the analyzed VLP system could be used in application scenarios where white light balance or luminaire color planning are also the goals.

Keywords: visible light communication (VLC); visible light positioning (VLP); free-space communication; RGB LED

check for updates

Citation: Martínez-Ciro, R.A.; López-Giraldo, F.E.; Luna-Rivera, J.M.; Ramírez-Aguilera, A.M. An Indoor Visible Light Positioning System for Multi-Cell Networks. *Photonics* **2022**, *9*, 146. https://doi.org/10.3390/photonics9030146

Received: 13 December 2021
Accepted: 7 February 2022
Published: 1 March 2022

1. Introduction

Indoor positioning systems (IPS) have been widely studied in the literature for different applications such as indoor navigation in museums and exhibition centers, tracking people or objects in indoor scenarios, robot movement control, location-based advertisement distribution in stores, etc. [1]. Some existing technologies have been used to provide indoor localization services, including Bluetooth, Wi-Fi, infrared ray, radio frequency identification, ultra-wideband, ZigBee, ultrasonic, and more recently, visible light communication (VLC). In particular, visible light positioning (VLP) is a VLC-based technology that has attracted more attention due to its high accuracy and low-cost implementation [2]. In recent years, VLC-based localization systems have already been proposed for application in healthcare facilities, indoor public spaces, shopping centers, underground mines, the Internet of Things (IoT), etc. [2–7]. Various methods can be adopted to build a VLP system, such as angle of arrival (AOA), time of arrival (TOA), and received signal strength (RSS). Although TOA requires strict synchronization between transmitting and receiving, AOA needs higher hardware requirements. On the other hand, RSS-based methods have attracted extensive attention for their high positioning accuracy, low cost, and simplicity in hardware. In this way, this paper adopts an RSS-based indoor localization solution [8–10].

In principle, a light detector-based VLP system uses a photodiode sensor to capture the optical signal from WLED lamps and utilizes the RSS information of WLED lamps for positioning calculation with a trilateration algorithm [11]. The adoption of WLEDs in lighting applications has yielded many VLP solutions in the literature. The advantages of WLEDs include a long lifetime, small size, low power consumption, and high efficiency [12,13]. A VLP solution based on WLEDs can be classified according to the number of LED lights used for positioning, i.e., a single LED or multiple LEDs. In 2013, Kim et al. proposed an RSS-based VLP system using a radio frequency (RF) carrier allocation technique with three WLEDs. The results of the experiments for a single-cell showed position error estimates of about 2.4 cm on average in an indoor space of $60 \times 60 \times 60$ cm^3 [14]. In 2016, Hsu et al. proposed an indoor visible light positioning experiment that combines the LED's ID positioning, RSS, radio frequency carrier allocation, and a solar cell as an optical receiver. This VLP system also uses three WLEDs in a single cell, which achieved centimeter-level positioning accuracy [15]. Another experimental VLP solution is presented in [16], based on linear interpolation, RF carrier, and three white LEDs. The results showed that the achieved positioning error is lower than 5 cm. The work of Xu et al. [17] used multiple photodiodes to help WLED position calculation with projective geometry and RSS indications. Their VLP system achieved a positioning error of 13 cm with an architecture based on two photodiodes and two WLEDs. In [18], Cai et al. used a particle swarm optimization (PSO) algorithm to perform a three-dimensional coordinate estimation in an indoor environment of $0.9 \times 0.9 \times 1.5$ m^3 with four WLEDs and one photodiode. Nevertheless, it is not advantageous to use PSO in a real-time VLP system with multiple cells due to the iterations required for the localization problem. In [19], Huang et al. employ received signal strength for a two-dimensional VLP system with a positioning accuracy of about 8 cm in a small $200 \times 60 \times 60$ cm^3 space. On the other hand, there are only few research works that have proposed a VLP architecture for a multi-cell area based on white LEDs [14–16,20–23]. For example, in [24], Little et al. proposed a multi-cell lighting testbed for a VLP system based on the RSS technique and radio frequency allocation. The testbed was constructed with 15 WLEDs in an indoor environment of $1.8 \times 3.9 \times 1.47$ m^3 with an average accuracy of 50 cm. However, this work did not provide simulation or experimental results. In addition, when the application scenario has a large coverage area, the complexity of the implementation could be high due to the multiple transmitter LEDs needed in the VLP system. In [25], a visible light positioning system is proposed for indoor Internet of Things. The simulation system is conducted with 4 cells and 16 WLEDs in a room size of $10 \times 10 \times 3$ m^3. A filter bank of multicarrier-based subcarrier multiplexing (FBNC-SCM) techniques was exploited to provide a high-speed data rate and high-accuracy positioning. However, Tx and Rx modulation and demodulation processes are very complex due to the multiple sub-processes such as the synchronization of all WLEDs, band and low-pass filters, inverse fast Fourier transform, quadrature amplitude modulation and others.

On the other hand, there are few existing works on multi-color transmission channels for VLP systems. Trichromatic WLEDs based on red–green–blue (RGB) LEDs have become promising in the VLP system because they offer the possibility to perform wavelength division multiplexing (WDM) and color shift keying (CSK) [26,27]. In [26], Vieira et al. proposed a VLP based on RGB LEDs with WDM, a double PIN photodetector with two UV light biased gates, the RSS technique, and the multilateration method. Additionally, an extra ultraviolet LED was added to the system for error control in the synchronization process of the transmitter and receiver. The VLP system performs different filtering processes and decodes encoded signals for recovering the transmitted data information. However, Vieira et al. [26] only presents a VLP architecture for one cell where the complexity is affected due to multiple processes. Furthermore, it does not provide an explicit expression to estimate the Euclidean distances of the VLP system based on RGB LEDs. Moreover, the work in [26] does not report the result of the evaluation of the localization error's performance.

In this paper, we propose for the first time an indoor VLP solution for a multi-cell network using RGB LEDs. The positioning system combines a frequency division multiplexing (FDM) scheme with an RSS-based trilateration method within a network with K cells. Each cell consists of three RGB LED transmitters and one photodiode detector located at the mobile user as the optical receiver. This method resembles the VLC system using color-shift keying (CSK) modulation, as proposed in the standard IEEE 802.15.7 [27–30]. Some important features of the CSK scheme are adapted to the localization problem in the VLP system of this work. Furthermore, we enable FDM signals on the CSK symbols to transmit the identification (ID) of the luminaries but also to mitigate inter-cell interference. A total of seven chromatic points are used in the VLC transmitter configuration. The expression of the Euclidean distance for the 7-CSK constellation is calculated according to the optical channel response and the power spectral density in the received signal. For the analysis of the VLP system, we adopted the VLC channel with line-of-sight (LOS) and non-line-of-sight (NLOS) components. The evaluation of the error performance is given as a function of the chromatic point transmitted by the RGB LED. Finally, the properties of the proposed positioning system are investigated using Monte Carlo simulations.

The sections to come are organized as follows. Section 2 presents the conventional VLP system model based on WLEDs. The proposed VLP system model is then introduced in Section 3 to include RGB LEDs. After that, the results are presented in Section 4, followed by the conclusions in Section 5.

2. VLP System Model Based on WLEDs

This section gives a brief overview of the operating principles of the existing VLP system models using WLEDs [14–16]. Although some research works in the literature consider multiple cells within the VLP architecture [14–16,20], they confine the simulation or experimental evaluations to the single-cell scenario. Therefore, let us first review the basic VLP model using WLEDs. Figure 1 presents a conventional single-cell architecture of the VLP system based on WLEDs for a two-dimensional (2D) location system [14,15,20].

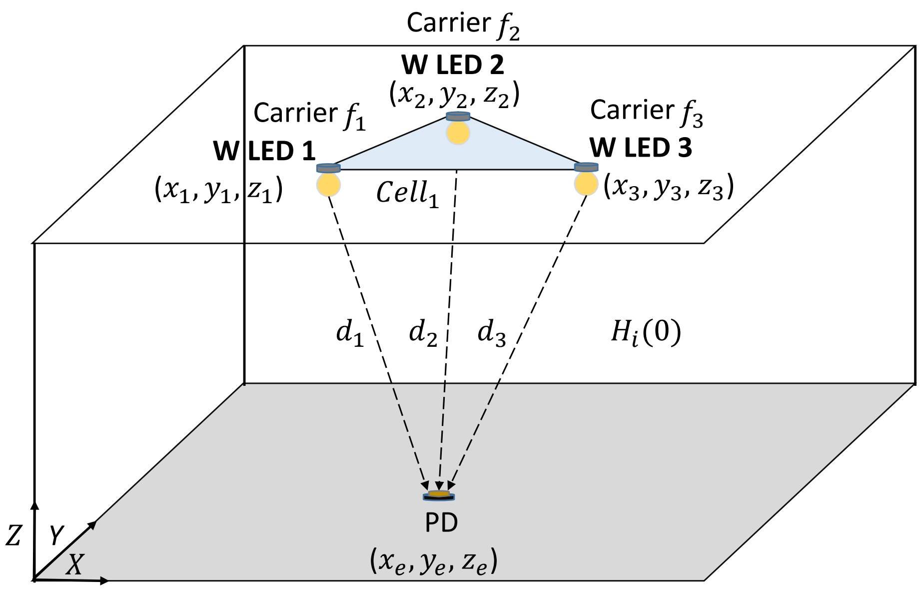

Figure 1. Architecture and geometric model of the VLP for one cell based on three WLEDs.

In this architecture, three WLEDs placed on the ceiling in a triangular configuration provide coverage for the cell. The principle of VLP is that each WLED transmits a unique signal that allows users to calculate their position. An optical receiver, such as a photodiode (PD), can use this information and a trilateration algorithm to calculate the location of the user.

The application of the trilateration method requires the signal of at least three WLEDs to calculate a 2D position of the user. It estimates the Euclidean distances d_i between the PD and each WLED position, which mathematically can be expressed as [14,15,20]:

$$d_i = \sqrt{(x_e - x_i)^2 + (y_e - y_i)^2 + (z_e - z_i)^2}, \tag{1}$$

where $(x_i,\ y_i,\ z_i)$ is the coordinate of the i-th WLEDs for $i = 1,2,3$, and $(x_e,\ y_e,\ z_e)$ is the PD position. The height of each WLED on the ceiling is the same; that is, $z_1 = z_2 = z_3 = Z$ and $z_e = 0$, where $(X,\ Y,\ Z)$ are the workspace dimensions. Then, the estimated 2D position, $\mathbf{X} = [x_e\ y_e]^T$, can be calculated by following a system of two linear equations. Such a system can be rewritten in a matrix form as follows [14,15]:

$$\mathbf{AX} = \mathbf{B}, \tag{2}$$

where

$$\mathbf{A} = \begin{bmatrix} x_2 - x_1 & y_2 - y_1 \\ x_3 - x_1 & y_3 - y_1 \end{bmatrix}, \quad \mathbf{X} = \begin{bmatrix} x_e \\ y_e \end{bmatrix}, \quad \text{and } \mathbf{B} = \begin{bmatrix} \frac{(d_1^2 - d_2^2 + x_2^2 + y_2^2 - x_1^2 - y_1^2)}{2} \\ \frac{(d_1^2 - d_3^2 + x_3^2 + y_3^2 - x_1^2 - y_1^2)}{2} \end{bmatrix}.$$

As previously mentioned in Section 1, several approaches can be used to calculate the Euclidean distances between the PD and the WLEDs, such as RSS, AOA, or TOA [14–16,20]. For the study of the VLP system proposed in this work, we take as reference the WLED-based VLP system presented by Constanzo et al. [20]. However, it should be noted that their model is useful for a VLP system with one cell. Therefore, in Constanzo et al., the Euclidean distances d_i are derived using the RSS method [20]. The FDM signals are adopted to divide the total bandwidth into a series of frequency sub-bands corresponding to each optical signal transmitted by WLEDs, P_{Topt}, with line-of sight (LOS). The light sensor transforms the incident optical power into a photovoltage, $x_i(t)$, conditioned and processed by electronic devices. The calculation of d_i between a WLED and the light sensor can be calculated as follows [20]:

$$d_i = \left(\frac{h_i^m (m+1) A \zeta P_{Topt} T(\psi) g(\psi)}{2\pi P_{ri}} \right)^{\frac{1}{m+2}}, \tag{3}$$

where h_i^m is the height between the i-th WLED and the PD receiver, with m as the order of the Lambertian radiation; A is the effective area of the photodiode; ζ is the calibrating factor; $T(\psi)$ is the gain of the optical filter; $g(\psi)$ is the receiver's optical concentrator gain; ψ is the angle of incidence with respect to the axis normal to the receiver surface; and P_{ri} is the receiver's optical power. Observe that m is related to $\phi/2$, which is the transmitter semi-angle, by $m = -ln2/ln(cos(\phi/2))$. In [20], they proposed to use the power spectral density of the photovoltage signal to estimate the received optical power values, as shown in the equation below (4).

$$Pr_i = \int_{f_i - \frac{f_i}{Q_i}}^{f_i + \frac{f_i}{Q_i}} PSD[x_i(t)]df, \tag{4}$$

where $PSD[\cdot]$ defines the power spectral density of the signal, and f_i and Q_i, for $i = 1,2,3$, are the carrier frequencies and the quality factors of peak filters, respectively.

Finally, the $(x_i,\ y_i,\ z_i)$ position of the luminaires is estimated by identifying binary codes or the frequency of the carrier signals associated with each ith transmitter [14–16,20].

3. Proposed VLP System Model Based on RGB LEDs

3.1. System Model

The conceptual multi-cell architecture of the proposed VLP system is presented in Figure 2. The coverage area of the indoor scenario is divided into K small cells, $cell_k$, for $k = 1, 2, 3 \ldots K$, each consisting of three RGB LEDs. Figure 3 shows the proposed method of the VLP system for a multi-cell network based on luminaire (L) RGB LEDs. This system includes three stages: (1) transmission protocol, (2) optical receiver, and (3) localization process. The first stage consists of the color coding based on the CIE 1931 chromaticity space, the FDM+DC technique, RGB LEDs as VLC transmitters, and optical channels based on the Lambertian model. The optical receiver is based on the Thorlabs' PDA36A light detector model, where we exploit the sensitivity response of the photodiode for estimating the RGB light power as a function of the photocurrent. This process is similar to those utilized in [27,31]. Then, the PDA36A converts the photocurrent into a voltage signal with a transimpedance amplifier. Finally, in the localization process, the FFT is applied to the voltage signal. After that, we suggest a mathematical procedure to calculate the Euclidean distance between the RGB LED emitter and the optical receiver. Next, the trilateration algorithm is used to estimate the receiver position.

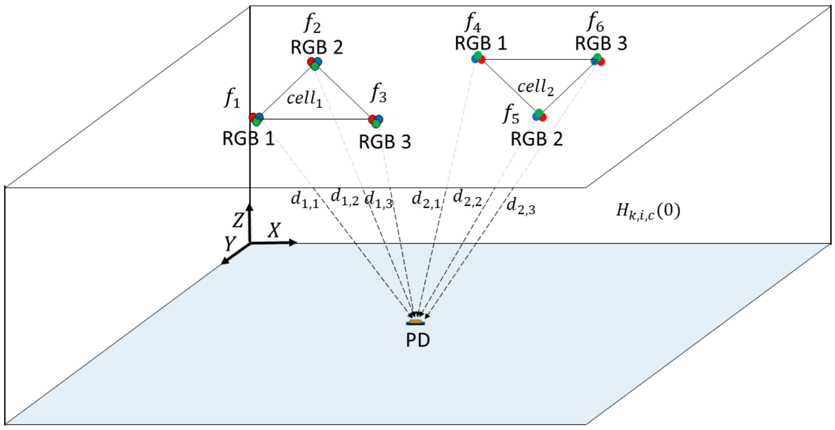

Figure 2. Muti-cell architecture of the proposed VLP system based on RGB LEDs.

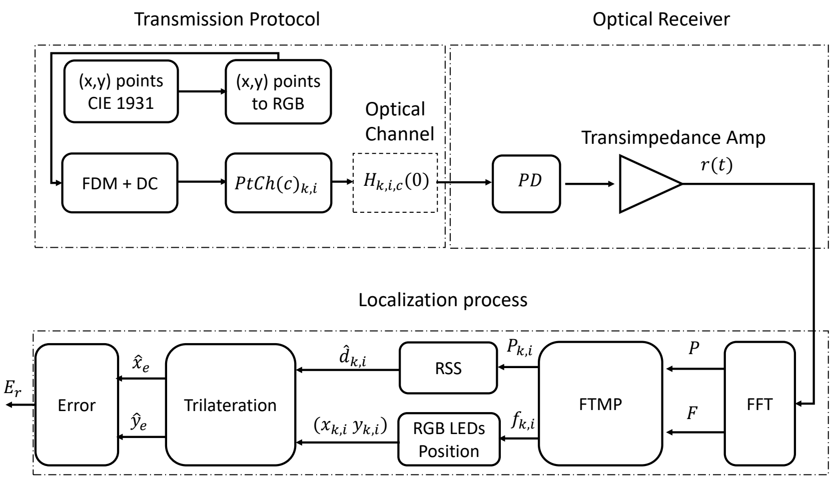

Figure 3. Proposed method for the RGB LED-based VLP system.

3.2. Transmission Protocol

In this section, we use the notation of $PtCh(c)_{k,i}$ to mention the transmitted optical power of some c channels for c = red (R), green (G) or blue (B), of the RGB LED i in $cell_k$. Note that all channels of an RGB LED transmit the same carrier signal. This is to take advantage of the maximum power emitted by each RGB channel. This is explained in detail in this section.

In every $cell_k$ of the network, each RGB LED will transmit a VLC signal with a unique identifier through a specific carrier frequency. Our approach allows for exploring the CIE 1931 RGB color space [32] to enable symbol mapping and constellation design in the same fashion as in color-shift keying (CSK) schemes [27]. Figure 4 illustrates an example of the color space constellation diagram for the 7-CSK modulation scheme with a triangular region denoted by the "RGB" vertices.

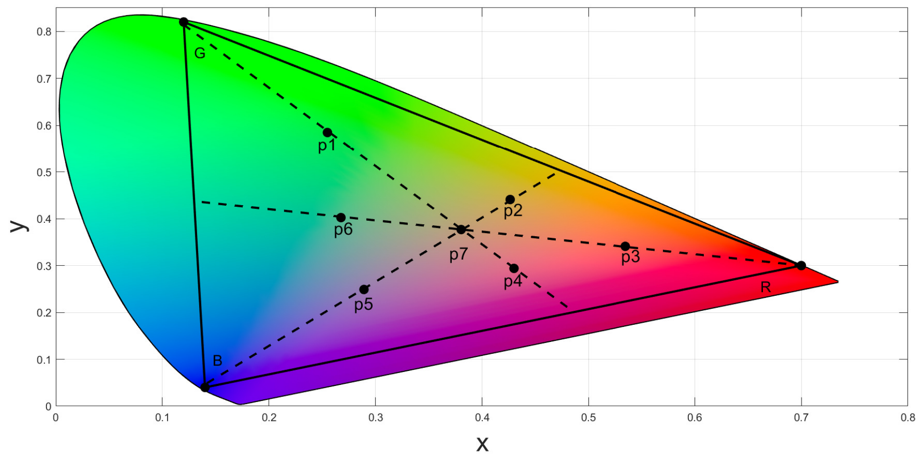

Figure 4. CIE 1931 chromatic points to explore in the VLP system based on RGB LEDs.

The transmitter of the VLP system is composed of multiple processes. The first process is the selection of the chromatic point on CIE 1931 space. This constellation point generates normalized optical powers for each RGB light channel. Then, these power levels are used to configure the FDM scheme and the direct current (DC) generation block. The signals generated by these systems (FDM + DC) modulate the bias current of the RGB LEDs. The FDM signal encodes the identifiers (ID) of each RGB LED through frequencies, and the DC signal configures each RGB LED to yield positive optical signals. This mechanism ensures that the RGB LED transmits the ID while maintaining color balance.

Specifically, the transmission protocol is defined as follows. First, we select one chromatic point on CIE 1931 color space (see Figure 4) for transmitter configuration. The chromatic point is represented by the normalized optical power vector $[P_r,\ P_g,\ P_b]^T$ through the Equation (5). Each chromatic point $(x_p,\ y_p)$ could be explored in the transmission of the carrier signals of the VLP system. Therefore, any constellation point (from P_1 to P_7) can be represented by the vector of optical powers

$$\mathbf{P} = \begin{bmatrix} P_r \\ P_g \\ P_b \end{bmatrix} = \begin{bmatrix} x_r & x_g & x_b \\ y_r & y_g & y_b \\ 1 & 1 & 1 \end{bmatrix}^{-1} \begin{bmatrix} x_p \\ y_p \\ 1 \end{bmatrix}, \quad (5)$$

where the ordered pairs $(x_r,\ y_r)$, $(x_g,\ y_g)$ and $(x_b,\ y_b)$ represent the color values $(x,\ y)$ associated with the peak wavelength of the sources of red, green, and blue light, respectively [27]. The optical power signals $[P_r\ P_g\ P_b]^T$ of ith RGB LEDs in each $cell_k$ are transmitted through the free space channel $H_{k,i,c}(0)$.

Using an FDM technique, the ith RGB LED in $cell_k$ will transmit its identification signal $PtCh(c)_{k,i}$ in a specific RF carrier wave with a modulation frequency $f_{k,i}$ through each particular channel c. Since the carrier wave exhibits signal variations from negative to positive values, a DC bias should be applied. Therefore, the carrier signals transmitted by each channel of the RGB LED are shown in Equation (6):

$$PtCh(c)_{k,i} = \frac{P_c PLED_c sin(2\pi f_{k,i} t) + 1)}{2}, \tag{6}$$

where P_c is the normalized optical power for channel c, and $PLED_c$ corresponds to the maximum emission optical power of the c channels of the LEDs. Notice that these optical powers will depend on the characteristics of the RGB LED used. The chromaticity of the light emitted by RGB LEDs is established through the aforementioned process. Following electrical-to-optical conversion, the optical signal is propagated through free space, where the channel DC gain of the visible light communication system, $H_{k,i,c}(0)$, is composed of an LOS and non-LOS (NLOS) component, such that $H_{k,i,c}(0) = H_{k,i,c}(LOS) + H_{k,i,c}(NLOS)$ [33]. This can be expressed by (7) [33]:

$$H_{k,i,c}(0) = \frac{(m+1)}{2\pi d_{k,i}^2} A cos_{k,i}^m(\phi) cos(\psi) T(\psi) g(\psi) + \frac{A}{A_{room}} \frac{\langle \rho_c \rangle}{1 - \langle \rho_c \rangle}, \tag{7}$$

where A_{room} is the room surface, and $\langle \rho_c \rangle$ expresses the average reflectivity of a given room. According to the definition of $\langle \rho_c \rangle$, we can adopt the $\langle \rho_r \rangle$, $\langle \rho_g \rangle$ and $\langle \rho_b \rangle$ values proposed in [34]. On the other hand, we use the definition in [20,35] for the LOS channel. They assume $cos(\psi) = cos(\phi)$ is also equal to $h_{k,i}/d_{k,i}$ for horizontal orientation. Equation (7) can be rewritten as:

$$H_{k,i,c}(0) = \frac{(m+1)}{2\pi d_{k,i}^{m+3}} A h^{m+1} T(\psi) g(\psi) + \frac{A}{A_{room}} \frac{\langle \rho_c \rangle}{1 - \langle \rho_c \rangle}. \tag{8}$$

3.3. Optical Receiver

We make use of only one photodetector to convert the optical signals received from the RGB channels, to an electrical photocurrent [30,31]. Then, the photocurrent signal is used for the PD positioning problem, considering RF identification and the RSS technique. Next, the receiver optical power $PrCh(c)$ for c channels in the $cell_k$ can be determined as follows:

$$PrCh(c) = \sum_{k=1}^{K} \sum_{i=1}^{3} PtCh(c)_{k,i} H_{k,i,c}(0). \tag{9}$$

We use a single photodiode as an optical receiver of the RGB signals, in a similar fashion to the CSK-based VLC system proposed in [27,31] for low complexity receivers. However, the photodiode transforms each component of the RGB light into a photocurrent signal $r(t)$ corrupted by additive Gaussian noise $n(t)$ (AWGN), as shown in Equation (10):

$$r(t) = G_{amp} S PrCh(c) R(\lambda_c) + n(t), \tag{10}$$

where G_{amp} corresponds to the transimpedance gain; S is the scale factor; and the scalars $R(\lambda_R)$, $R(\lambda_G)$ and $R(\lambda_B)$ determine the photodiode responsivity associated with each red, green and blue wavelength, respectively [36]. Note that, the receiver optical power $PrCh(c)$ is made up of several carrier signals on different RGB light channels. Such a scheme takes advantage of the FDM structure by avoiding the use of multiple photodiodes with RGB filters in the receiver. Therefore, the localization process requires decomposing the FDM signal at the receiver by applying the fast Fourier transform (FFT) on the RGB optical power signal received at the PD. This process allows for estimating the power-spectral density (PSD) of the received power signal, as shown in Equation (11):

$$PSD[PrCh(c)R(\lambda_c)] = PSD\left[\frac{r(t)}{G_{amp} S}\right]. \tag{11}$$

3.4. Localization

In this section, we describe the localization stage for the VLP system based on RGB LEDs. This process is mainly divided into two phases. At first, the Euclidean distances between the RGB LED transmitters and the optical receiver are computed by processing the FFT of the voltage signal generated with the light sensor and using an RSS-based method. A simple frequency identification algorithm is used for the RGB LED position estimation. The second phase performs the trilateration algorithm that uses the Euclidean distance and the RGB LED position parameters to estimate the receiver location.

Figure 5 shows an example of the received RGB power vector for a VLP system with two cells. In this example, we use six carrier frequencies to modulate the RGB LEDs with $Pr_{k,i}$ as the maximum value of the received optical power for the R, G and B channels of the $cell_k$ with $k = 1, 2$. Considering Equation (11), we can apply the integral to the PSD signal in the interval $f_{k,i} \pm \Delta$ to calculate $Pr_{k,i}$, as it is shown in Equation (12):

$$Pr_{k,i} = R(\lambda_c)PtCh(c)_{k,i}H_{k,i,c}(0) = max\left(\int_{f_{k,i}-\Delta}^{f_{k,i}+\Delta} PSD\left[\frac{r(t)}{G_{amp}S}\right]df\right), \tag{12}$$

where $f_{k,i}$ represents the carrier frequency of luminaire i in cell k, and $\pm\Delta$ is the frequency limits used to delimit the area of peak powers $Pr_{k,i}$. It should be noted that only three optical signals are needed for the two-dimensional positioning problem. Consequently, a basic search algorithm is carried out on the signal $Pr_{k,i}$ to identify the three-maximum powers (TMP) and the associated frequencies. The Euclidean distance $\hat{d}_{k,i}$ is then estimated by measuring the received signal strength (RSS). Note that $Pr_{k,i}$ and $\hat{d}_{k,i}$ are scalar values. Therefore, we only consider the root mean square (RMS) values of the optical signal transmitted by each channel c, with $Ptrms(c)_{k,i} = RMS(PtCh(c)_{k,i})$. In addition, it should be noted that each RGB LED transmits the same carrier signal through the c channels. Therefore, the total contribution of the RMS optical powers emitted by the c channels was considered as a summation. Consequently, and substituting Equation (8) in (12), the Euclidean distance is estimated as shown in Equation (13):

$$\hat{d}_{k,i} = \sqrt[m+3]{\frac{(m+1)\sum_{c=R}^{B}\left(R(\lambda_c)Ptrms(c)_{k,i}\right)Ah^{m+1}T(\psi)g(\psi)}{2\pi\left(Pr_{k,i}-\sum_{c=R}^{B}\left(R(\lambda_c)Ptrms(c)_{k,i}H_{k,i,c}(NLOS)\right)\right)}}. \tag{13}$$

On the other hand, the frequencies $f_{k,i}$ are used to identify the coordinate $(x_{k,i},\ y_{k,i})$ of luminaire i of the $cell_k$. Finally, we perform the trilateration algorithm with $\hat{d}_{k,i}$ and $(x_{k,i},\ y_{k,i})$ to estimate the position of PD $(\hat{x}_e,\ \hat{y}_e)$ using Equation (2).

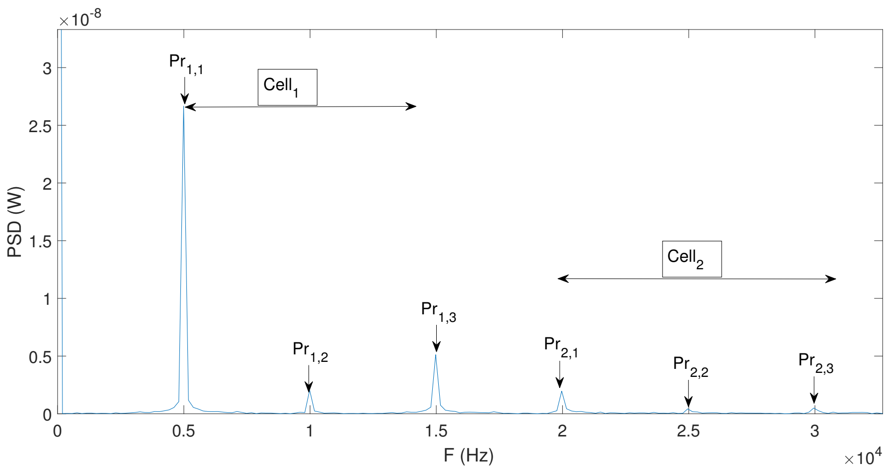

Figure 5. Power spectral density on the RGB optical power vector for VLP-based RGB LEDs

4. Simulation Results and Discussion

In this section, for the various color points addressed in Section 3, we evaluate the indoor positioning performance under the LOS and NLOS VLC channel model. We use the Monte Carlo method to evaluate the positioning error of the proposed RGB LED- based VLP system. The simulation results are presented using different mobile locations and chromatic points for the RGB LEDs. The chromaticity coordinates on the CIE 1931 of the red, green, and blue LEDs were $(0.70,\ 0.30)$, $(0.19,\ 0.78)$, and $(0.09,\ 0.13)$. We explored a total of seven color points p_1 to p_7 for the RGB LED configuration. Each chromatic point was evaluated in the VLP system. The specific chromatic point $(x_p,\ y_p)$ and the normalized optical power vector $[P_r\ P_g\ P_b]^T$ are shown in Table 1. It should be noted that, each optical power vector satisfies the rule $P_r + P_g + P_b = 1$ for the CIE 1931 standard [32]. The simulated VLP system considers two cells with a total of six RGB LEDs, as it is shown in Figure 2. This architecture allows us to validate the proposed method presented in Figure 3. We highlight that this architecture can be extended for multiple cells depending on the area of the application scenario.

Table 1. Color coordinates and normalized optical power vector.

Chromatic Point	$(x_p,\ y_p)$	$[P_r\ P_g\ P_b]^T$
p_1	$(0.2549,\ 0.5849)$	$[0.2274\ 0.6228\ 0.1498]^T$
p_2	$(0.4264,\ 0.4410)$	$[0.5236\ 0.3396\ 0.1369]^T$
p_3	$(0.5349,\ 0.3411)$	$[0.7105\ 0.1492\ 0.1403]^T$
p_4	$(0.4310,\ 0.2940)$	$[0.5233\ 0.1512\ 0.3255]^T$
p_5	$(0.2892,\ 0.2490)$	$[0.2728\ 0.1770\ 0.5502]^T$
p_6	$(0.2676,\ 0.4024)$	$[0.2416\ 0.3841\ 0.3743]^T$
p_7	$(0.3804,\ 0.3769)$	$[0.4395\ 0.2854\ 0.2751]^T$

The parameters used in the simulations of the VLP system are summarized in Table 2. The ceiling is fixed at a height of 2.2 m from the receiver (photodiode), assuming that in real applications, the user could carry the receiver at a height (z_e) of 0.8 m from the floor. We divide the space in the X–Y plane into a 4×7 grid. Each point of the grid indicates a test spot and the real coordinates $(x_e,\ y_e)$ of the receiver. For the VLC channel model, we use the definition in [33] for the NLOS channel and we can adopt the average reflectivity proposed in [34]. However, the reflection coefficients presented in [34] were estimated considering the power spectrum of a WLED as an emission source. Consequently, the values for $\langle\rho_r\rangle$, $\langle\rho_g\rangle$ and $\langle\rho_b\rangle$ of the RGB LED adopted in this article are approximate values of the R, G and B components of the WLED proposed by [34]. Next, we estimated the received RF power with the power spectral density according to Equation (11), where the maximum value of the received optical power for R, G and B channels were computed with Equation (12). After solving the Equations (13) and (2), the positioning result can be obtained. Please note that the positioning error is then defined as the Euclidean distance between the actual coordinate $(x_e,\ y_e)$ and the estimated mobile receiver position $(\hat{x}_e,\ \hat{y}_e)$ on all the test points.

Figures 6 and 7 show the results of the positioning errors obtained for all chromatic points $(p_1$–$p_7)$. All chromatic points showed similar localization error performance. It can be seen that the lowest positioning errors were obtained for p_6 (see Figure 7b) (on average 1.96 cm), and the highest errors for p_5 (see Figure 7a) (on average 2.13 cm). This small variation in localization error could be related to the effect of the NLOS component and photodetector responsivity for some wavelengths on the performance of the VLP system.

Table 2. Simulation parameters.

Parameters	Value	Parameters	Value
Dimension space	$X = 6$ $Y = 3$ $Z = 3$ m	RGB LED optical power for channel	3.333 W
RGB 1 coordinates	(0.75, 0.75, 3) m	$f_{1,1}$	5 kHz
RGB 2 coordinates	(1.50, 2.25, 3) m	$f_{1,2}$	10 kHz
RGB 3 coordinates	(2.25, 0.75, 3) m	$f_{1,3}$	15 kHz
RGB 4 coordinates	(3.75, 2.25, 3) m	$f_{2,1}$	20 kHz
RGB 5 coordinates	(4.50, 0.75, 3) m	$f_{2,2}$	25 kHz
RGB 6 coordinates	(5.25, 2.25, 3) m	$f_{2,3}$	30 kHz
RGB LED half-power angle	$\phi/2 = 60^{\circ}$	$R(\lambda_R)$	0.41 A/W
Detector area	$A = 13^{-6}$ m^2	$R(\lambda_G)$	0.2 A/W
G_{amp}	0.75^6 V/A	$R(\lambda_B)$	0.12 A/W
Scale factor	$S = 0.5$	Noise (RMS)	340^{-6} V
$T(\psi)$	1	$g(\psi)$	1
Sampling rate	96,000 kHz	FFT points	1500
Δ	300 Hz	$\langle\rho_r\rangle$	0.0733
$\langle\rho_g\rangle$	0.0450	$\langle\rho_b\rangle$	0.0558
A_{room}	90 m^2	m	1

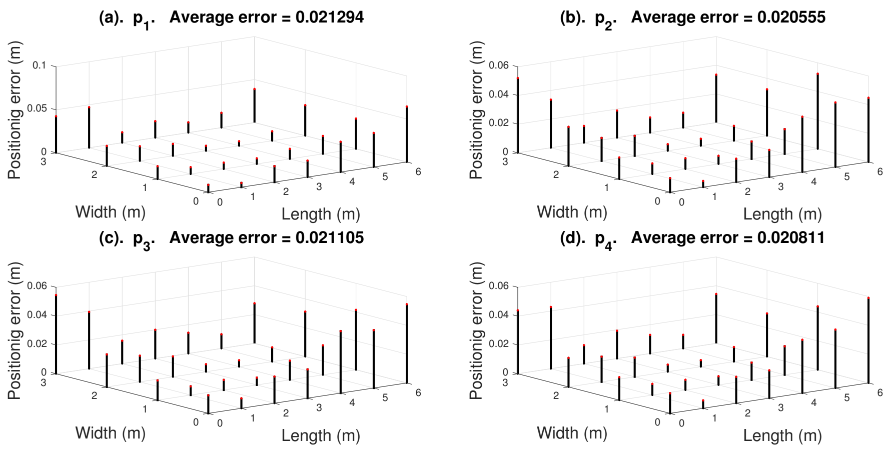

Figure 6. Positioning error for chromatic points p_1 to p_4.

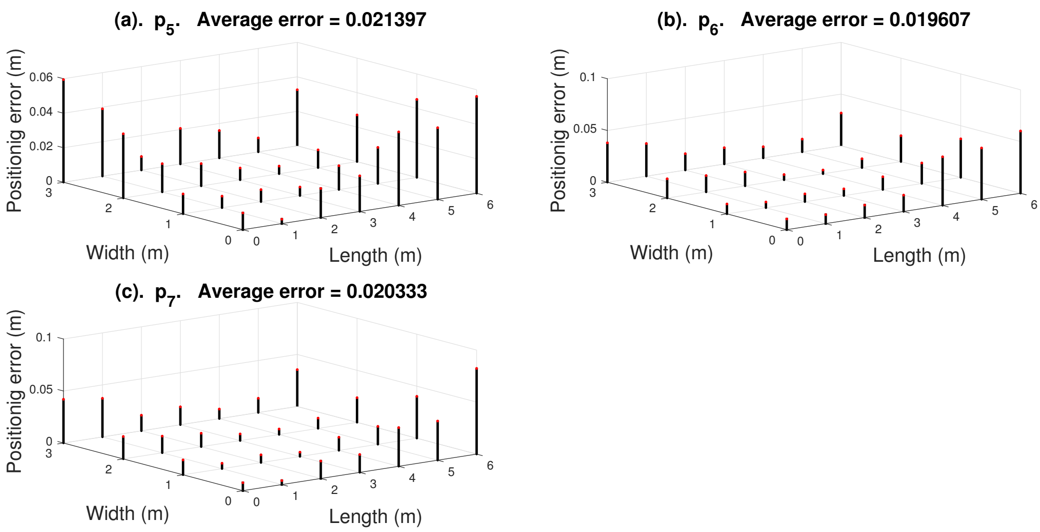

Figure 7. Positioning error for chromatic points p_5 to p_7.

The performance for some of the chromatic points showed larger errors at the sides or corners of the room. This could be caused by the low optical power provided by the RGB channels on the surface of the photodiode. However, the results of the maximum average localization error of 2.13 cm show a good performance of the VLP system based on RGB LEDs. These results validate the proposed method and the derived equations in the parameter estimation process. We remark that any chromatic point in the CIE 1931 space could be exploited in the design of the VLP system based on RGB LEDs. Nevertheless, the color balance should be set according to the lighting requirements of the application scenario. For example, the p_7 color point (see Figure 7c) can be used if the application scenario requires white light balance. Otherwise, the chromaticity of the light contributions by points p_1 to p_6 can be useful in other scenarios such as museums, where the color planning of the luminaires can be configured for some artwork or specimens.

The RGB LED-based VLP system showed good error performance as compared to existing WLED-based VLP architectures [14,16,17,19,24]. Additionally, we note that in VLP architecture based on RGB LEDs, the signal-to-noise ratio could be positively impacted by transmitting the same carrier signal over the RGB channels. Our proposed VLP system also allows us to explore the color temperature of the RGB luminaire, considering the CIE 1931 standard, which is not possible with WLED because the color temperature is fixed. However, it is important to note that the VLP architecture based on RGB LEDs requires more hardware components than that based on WLEDs. On the other hand, our VLP system proposes cells based on three RGB LEDs, where the mathematical expression to estimate the Euclidean distances were derived. Our system requires fewer components than the VLP architecture proposed by [26] because they employed an additional ultraviolet LED in the VLP system based on RGB LEDs. Additionally, they do not provide an explicit expression for estimating the Euclidean distances.

5. Conclusions

In this work, we presented a novel design of a VLP system based on RGB LEDs considering multiple cells and a frequency division multiplexing scheme. We proposed indoor positioning adopting VLC based on the LOS and NLOS environment, which was investigated by simulation. We propose a new method to estimate the position of the mobile user receiver within a multiple-cell coverage network, suggesting different possible sets of chromatic points in CIE 1931 space for the configuration of the transmitters. This system adopted the RSS and trilateration techniques that combine frequency identification for the localization problem. The proposed design achieves a simpler and more flexible transmitter position identification than using frequency identification combined with the modulation technique. The resulting VLP system is able to perform lighting system chromaticity control, visible light communication and indoor positioning simultaneously. A proof-of-concept example was developed to test this approach. We emulated a practical indoor scenario by setting the height of the room at 3 m with a distance of 2.2 m between the RGB LEDs, on the ceiling of the room, and the photodiode receiver. In addition, numerical simulations have been carried out to validate the analytical expression derived for the Euclidean distance vector. These results showed good agreement between the experimental simulation and the theoretical analysis. We observed a high positioning accuracy performance for the chromatic point p_5. However, the average positioning error for all chromatic points was less than 2.2 cm. The proposed VLP system would be useful for various indoor location-based applications. The chromatic point p_7 could be recommended for an application scenario in which the lighting requires white light balance. More importantly, this VLP-based RGB LED maintains compatibility with the use of the CIE 1931 standard.

Author Contributions: Conceptualization, J.M.L.-R. and R.A.M.-C.; formal analysis, J.M.L.-R. and R.A.M.-C.; investigation, F.E.L.-G., R.A.M.-C. and A.M.R.-A.; software, R.A.M.-C.; writing–original draft preparation, R.A.M.-C. and F.E.L.-G.; writing–review and editing, F.E.L.-G., A.M.R.-A. and J.M.L.-R. All authors have read and agreed to the published version of the manuscript.

Funding: This research received no external funding.

Institutional Review Board Statement: Not applicable.

Informed Consent Statement: Not applicable.

Data Availability Statement: Not applicable.

Acknowledgments: This research and the APC were funded by Instituto Tecnológico Metropolitano [grant PCI 20203], Colombia.

Conflicts of Interest: The authors declare no conflict of interest.

References

1. Zafari, F.; Gkelias, A.; Leung, K.K. A Survey of Indoor Localization Systems and Technologies. *IEEE Commun. Surv. Tutor.* **2019**, *21*, 2568–2599. [CrossRef]
2. Zhuang, Y.; Cao, Y.; Wu, Y.; Member, S.; Thompson, J.; Haas, H. A Survey of Positioning Systems Using Visible LED Lights. *IEEE Commun. Surv. Tutor.* **2018**, *20*, 1963–1988. [CrossRef]
3. Yasir, M.; Ho, S.; Vellambi, B. Indoor Position Tracking Using Multiple Optical Receivers. *J. Lightwave Technol.* **2016**, *34*, 1166–1176. [CrossRef]
4. Rahman, A.B.M.M.; Li, T.; Wang, Y. Recent Advances in Indoor Localization via Visible Lights: A Survey. *Sensors* **2020**, *20*, 1382. [CrossRef] [PubMed]
5. Chen, P.; Pang, M.; Che, D.; Yin, Y.; Hu, D.; Gao, S. A Survey on Visible Light Positioning from Software Algorithms to Hardware. *Wirel. Commun. Mob. Comput.* **2021**, *2021*, 9739577. [CrossRef]
6. Almadani, Y.; Ijaz, M.; Rajbhandari, S.; Raza, U.; Adebisi, B. Applications of Visible Light Communication for Distance Estimation: a Short Survey. In Proceedings of the 2019 IEEE Jordan International Joint Conference on Electrical Engineering and Information Technology (JEEIT), Amman, Jordan, 9–11 April 2019; pp. 261–265. [CrossRef]
7. Chaudhary, N.; Alves, L.N.; Ghassemblooy, Z. Current Trends on Visible Light Positioning Techniques. In Proceedings of the 2019 2nd West Asian Colloquium on Optical Wireless Communications (WACOWC), Tehran, Iran, 27–28 April 2019; pp. 100–105. [CrossRef]
8. Stevens, N.; Steendam, H. Magnitude of the Distance Estimation Bias in Received Signal Strength Visible Light Positioning. *IEEE Commun. Lett.* **2018**, *22*, 2250–2253. [CrossRef]
9. Guo, X.; Ansari, N.; Hu, F.; Shao, Y.; Elikplim, N.R.; Li, L. A survey on fusion-based indoor positioning. *IEEE Commun. Surv. Tutor.* **2020**, *22*, 566–594. [CrossRef]
10. Luo, J.; Fan, L.; Li, H. Indoor Positioning Systems Based on Visible Light Communication: State of the Art. *IEEE Commun. Surv. Tutor.* **2017**, *19*, 2871–2893. [CrossRef]
11. Karunatilaka, D.; Zafar, F.; Kalavally, V.; Parthiban, R. LED Based Indoor Visible Light Communications: State of the Art. *IEEE Commun. Surv. Tutor.* **2015**, *17*, 1649–1678. [CrossRef]
12. Do, T.H.; Yoo, M. An in-depth survey of visible light communication based positioning systems. *Sensors* **2016**, *16*, 678. [CrossRef]
13. Popoola, O.; Sinanović, S.; Popoola, W.; Ramirez, R. Optical Boundaries for LED-Based Indoor Positioning System. *Computation* **2019**, *7*, 7. [CrossRef]
14. Kim, H.S.; Kim, D.R.; Yang, S.H.; Son, Y.H.; Han, S.K.; Liao, X.; Lin, K.; Chen, Y. An Indoor Visible Light Communication Positioning System Using a RF Carrier Allocation Technique. *J. Lightwave Technol.* **2013**, *31*, 131–144. [CrossRef]
15. Hsu, C.W.; Wu, J.T.; Wang, H.Y.; Chow, C.W.; Lee, C.H.; Chu, M.T.; Yeh, C.H. Visible Light Positioning and Lighting Based on Identity Positioning and RF Carrier Allocation Technique Using a Solar Cell Receiver. *IEEE Photonics J.* **2016**, *12*, 1–7. [CrossRef]
16. Wu, Y.C.; Hsu, K.L.; Liu, Y.; Hong, C.Y.; Chow, C.W.; Yeh, C.H.; Liao, X.L.; Lin, K.H.; Chen, Y.Y. Using Linear Interpolation to Reduce the Training Samples for Regression Based Visible Light Positioning System. *IEEE Photonics J.* **2020**, *12*, 1–5. [CrossRef]
17. Xu, W.; Wang, J.; Shen, H; Zhang, H.; You, X. Indoor Positioning for Multiphotodiode Device Using Visible-Light Communications. *IEEE Photonics J.* **2016**, *8*, 1–11.
18. Cai, Y.; Guan, W.; Wu, Y.; Xie, C.; Chen, Y.; Fang, L. Indoor High Precision Three-Dimensional Positioning System Based on Visible Light Communication Using Particle Swarm Optimization. *IEEE Photonics J.* **2017**, *9*, 1–20. [CrossRef]
19. Huang, N.; Gong, C.; Luo, J.; Xu, Z. Design and Demonstration of Robust Visible Light Positioning Based on Received Signal Strength. *J. Lightwave Technol.* **2020**, *38*, 5695–5707. [CrossRef]
20. Costanzo, A.; Loscri, V. Error compensation in indoor positioning systems based on software defined visible light communication. *Phys. Commun.* **2019**, *34*, 235–245. [CrossRef]
21. Chen, Y.; Zheng, H.; Liu, H.; Han, Z.; Ren, Z. Indoor High Precision Three-Dimensional Positioning System Based on Visible Light Communication Using Improved Hybrid Bat Algorithm. *IEEE Photonics J.* **2020**, *12*, 1–13. [CrossRef]
22. Alam, F.; Parr, B.; Mander, S. Visible Light Positioning Based on Calibrated Propagation Model. *IEEE Sens. Lett.* **2019**, *3*, 1–4. [CrossRef]
23. Anastou, A.C.; Delibasis, K.K.; Boulogeorgos, A.A.; Sandalidis, H.G.; Vavoulas, A.; Tasoulis, S.K. A Low Complexity Indoor Visible Light Positioning Method. *IEEE Access* **2021**, *9*, 57658–57673. [CrossRef]
24. Little, T.; Rahaim, M.; Abdalla, I.; Lam, E.; Mcallister, R.; Vegni, A. A multi-cell lighting testbed for VLC and VLP. In Proceedings of the 2018 Global LiFi Congress, Paris, France, 8–9 February 2018; Volume 1, pp. 1–6.

25. Yang, H.; Zhong, W.; Chen, C.; Alphones, A.; Du, P.; Zhang, S.; Xie, X. Coordinated Resource Allocation-Based Integrated Visible Light Communication and Positioning Systems for Indoor IoT. *IEEE Trans. Wirel. Commun.* **2020**, *19*, 4671–4684. [CrossRef]
26. Vieira, M.A.; Vieira, M.; Louro, P.; Mateus, L.; Vieira, P. Indoor positioning system using a WDM device based on a-SiC:H technology. *J. Lumin.* **2017**, *191*, 135–138. [CrossRef]
27. Martínez Ciro, R.A.; López Giraldo, F.E.; Betancur Perez, A.F.; Luna Rivera, J.M. Design and Implementation of a Multi-Colour Visible Light Communication System Based on a Light-to-Frequency Receiver. *Photonics* **2019**, *6*, 42. [CrossRef]
28. IEEE Computer Society Sponsored by the IEEE Standards Association: IEEE Standard for Local and Metropolitan Area Networks—Part 15.7: Short-Range Wireless Optical Communication Using Visible Light. September 2011. Available online: https://standards.ieee.org/findstds/standard/802.15.7-2011.html (accessed on 27 November 2018).
29. Mendes Matheus, L.E.; Borges Vieira, A.; Vieira, L.F.; Vieira, M.A.; Gnawali, O. Visible Light Communication: Concepts, Applications and Challenges. *IEEE Commun. Surv. Tutor.* **2019**, *21*, 3204–3237. [CrossRef]
30. Martínez Ciro, R.A.; López Giraldo, F.E.; Betancur Perez, A.F.; Luna Rivera, M. Characterization of Light-To-Frequency Converter for Visible Light Communication Systems. *Electronics* **2018**, *7*, 165. [CrossRef]
31. Luna-Rivera, J.M.; Suarez-Rodriguez, C.; Guerra, V.; Perez-Jimenez, R.; Rabadan-Borges, J.; Rufo-Torres, J. Low-complexity colour-shift keying-based visible light communications system. *IET Optoelectron.* **2015**, *9*, 191–198. [CrossRef]
32. CIE-1931, International Commission on Illumination, Colorimetry—Part 3: CIE Tristimulus Values, ISO 11664-3:2012(E)/CIE S014-3/E:2011. Available online: http://www.cie.co.at/publications/colorimetry-part-3-cie-tristimulus-values (accessed on 20 October 2020).
33. Zhang, X.; Duan, J.; Fu, Y.; Shi, A. Theoretical accuracy analysis of indoor visible light communication positioning system based on Received Signal Strength Indicator. *J. Lightwave Technol.* **2014**, *32*, 4180–4186. [CrossRef]
34. Lee, K.; Park, H.; Barry, J. Indoor channel characteristics for visible light communications. *IEEE Commun. Lett.* **2011**, *15*, 217–219. [CrossRef]
35. Plets, D.; Bastiaens, S.; Martens, L.; Joseph, W. An Analysis of the Impact of LED Tilt on Visible Light Positioning Accuracy. *Electronics* **2019**, *8*, 389. [CrossRef]
36. THORLABS, PDA36A(-EC) Si Switchable Gain Detector. Available online: https://www.thorlabs.com/thorproduct.cfm?partnumber=PDA36A-EC (accessed on 11 January 2021).